Quantum time correlation functions from complex time Monte Carlo simulations: A maximum entropy approach

Goran Krilov, Eunji Sim, and B. J. Berne
Department of Chemistry, Columbia University, 3000 Broadway, New York, New York 10027

(Received 13 July 2000; accepted 19 October 2000)

We present a way of combining real-time path integral Monte Carlo simulations with a maximum entropy numerical analytic continuation scheme in a new approach for calculating time correlation functions for finite temperature many body quantum systems. The real-time dynamics is expressed in the form of the symmetrized time correlation function, which is suitable for Monte Carlo methods, and several simulation techniques are presented for evaluating this function accurately up to moderate values of time. The symmetrized time correlation function is then analytically continued in combination with imaginary time data to obtain the real-time correlation function. We test this approach on several exactly solvable problems, including two one-dimensional systems, as well two cases of vibrational relaxation of a system coupled to a dissipative environment. The computed time correlation functions are in good agreement with exact results over several multiples of the thermal time $\beta\hbar$, and exhibit a significant improvement over analytic continuation of imaginary time correlation functions. Moreover, we show how the method can be systematically improved. © *2001 American Institute of Physics.*
[DOI: 10.1063/1.1331613]

I. INTRODUCTION

The last two decades have witnessed tremendous advances in the use of computer simulations as an efficient tool for predicting the properties of complex systems of classically interacting particles. Stochastic methods, such as Monte Carlo integration[1] (MC) have been an invaluable tool in predicting thermodynamic properties of large molecular systems. Other methods, based on the integration of classical equations of motion, also known as molecular dynamics[2,3] (MD) have been equally useful. In addition to allowing one to compute equilibrium properties by virtue of the ergodicity theorem, trajectories generated in molecular dynamics simulations can be used to predict time-dependent quantities as well. This feature is especially important, since many properties that are accessible to experiment are of the time-dependent nature. These include quantities such as transport coefficients, inelastic light and neutron scattering cross sections, dipole relaxation times, and reaction rates.

The experimental methods used to measure the above mentioned quantities share a common characteristic, that is they monitor the response of the system to a perturbation caused by an external field weakly coupled to it. In this regime, the dynamics of the system is adequately described by the linear response theory, which implies that the measured dynamic properties can be expressed in terms of time-correlation functions of the corresponding dynamic operators.[4] For systems evolving under the laws of classical mechanics, time-correlation functions can be computed from a canonical ensemble of the system's trajectories. These in turn are readily available from MD simulations.

In part due to the success of computer simulations in describing classical systems, great efforts have been made to develop simulation techniques for quantum mechanical systems as well. As a result, significant progress has been made in the use of stochastic methods in computing time-independent properties of quantum system. One stochastic method is diffusion Monte Carlo (DMC) [or quantum Monte Carlo[5–7] (QMC)] for calculation of the zero-temperature ground state properties. Other methods based on Feynman's path integral formulation of statistical mechanics,[8] known as path integral Monte Carlo[9] (PIMC) and path integral molecular dynamics[10] (PIMD) are used to calculate finite temperature equilibrium properties. These approaches have allowed accurate calculations for very large many-body quantum systems.

In contrast, simulating time evolution of finite temperature many body quantum mechanical systems has proven to be a formidable problem, and progress in this area has been much more modest. Feynman has pointed out that this problem is NP complete and suggested that quantum computers offer a solution.[11] Due to system size, basis-set methods and wave-packet propagation techniques used to solve the time dependent Schrödinger equation are not applicable. This leaves path integral methods as the only feasible alternative. However, in contrast to equilibrium properties, computation of time-dependent canonical averages using path integrals requires evaluation of multidimensional integrals over rapidly oscillating exponentials due to the presence of real-time propagators. Therefore, in this case stochastic methods based on importance sampling are inefficient and lead to statistical errors which grow exponentially with time. This is known as the ''sign problem,'' and is the primary obstacle to the use of computer simulations in calculating quantum time-correlation functions.

Numerous attempts have been made to partially alleviate

or suppress the sign problem. Most of these are based on the use of stationary phase filtering,[12–17] optimized reference systems,[18–20] and more recently renormalization techniques.[21–24] Likewise semiclassical methods such as SC-IVR, [25–30] and quasiclassical methods, such as centroid molecular dynamics[31–33] (CMD) have been successfully applied to systems in which quantum effects play a moderate role. While these methods introduce a great improvement over direct sampling of real-time path integrals, they nonetheless suffer from other limitations, and are in many cases applicable only to certain systems and system sizes. A good review of these methods can be found elsewhere.[34]

Another approach is based on computing quantum time-correlation functions by numerical analytic continuation of imaginary-time correlation functions, which are readily obtained from PIMC, to real time. The analytic continuation involves a numerical inversion of a Laplace transform, an extremely unstable operation, and requires the use of special techniques such as maximum entropy (ME) or singular value decomposition (SVD) to control the instability. In particular the ME method was successfully used to compute absorption spectra[35–38] and more recently, accurate quantum reaction rates.[39] Generally, this approach was found to adequately describe systems in which quantum coherences dissipate rapidly.

Still, the method has several limitations. The imaginary time data need to be determined with high accuracy in order to ensure the stability of the analytic continuation which requires long and expensive PIMC simulations. Even then, there can be many different real-time decays that are in agreement with the same imaginary time data within the statistical uncertainty. Another difficulty is that in imaginary time, the entire time domain is folded onto a small region of the imaginary time axis (between 0 and $\beta\hbar$), which further contracts with increasing temperature.

In a recent paper[40] we showed how approximate real-time data obtained from centroid molecular dynamics can be used within the context of ME numerical analytic continuation. The principal drawback of such an approach is that CMD is exact only for systems with purely harmonic interactions, and the deviations from the exact results can be quite severe for systems with very anharmonic interactions.

In this paper we present a way of combining the numerical analytic continuation approach with the real-time path integral simulations as a feasible method for computing quantum time correlation functions. Such an approach was recently suggested by Kim and Doll[41] as a way to improve the quality of analytic continuation methods. In Sec. II we present a symmetrized form of the time correlation function suitable for PIMC simulations, and in Sec. III discuss the simulation methods used. In Sec. IV we formulate the analytic continuation problem, and briefly outline the maximum entropy method used to perform it in Sec. V. We present the results for several test systems in Sec. VI. We conclude in Sec. VII.

II. SYMMETRIZED TIME CORRELATION FUNCTION

A general quantum time correlation function is given by

$$C_{AB}(t)=\langle A(0)B(t)\rangle=\frac{1}{Z}\mathrm{Tr}(e^{-\beta H}Ae^{iHt/\hbar}Be^{-iHt/\hbar}), \tag{1}$$

where A and B are quantum mechanical operators corresponding to measurable observables, H is the Hamiltonian of the system, and $\beta=1/kT$ is the inverse temperature. For reasons of simplicity, in this work we study autocorrelation functions of operators which are a function of position only, $A=B=A(x)$. We use one-dimensional notation for clarity, and generalization to multidimensional space is straightforward. In the position representation, Eq. (1) takes the form

$$C_{AA}(t)=\frac{1}{Z}\int dxdx'dx''dx''A(x')A(x'')\langle x|^{-\beta H}|x'\rangle \times\langle x'|e^{iHt/\hbar}|x''\rangle\langle x''|e^{-iHt/\hbar}|x\rangle. \tag{2}$$

Direct application of the path integral formalism to Eq. (2) would result in integrals over imaginary time paths connecting the states x' and x and pairs of forward and backward real-time paths, connecting x and x'' and x'' and x, respectively. One should note that the latter two have no positive definite weights due to the presence of real-time propagators with purely imaginary phases. As a result, stochastic importance sampling methods cannot be used to evaluate these integrals directly. Attempts to use stationary phase filtering techniques which introduce artificial positive definite weights have met with limited success.[14–17]

A form that appears much more suitable is the symmetrized time correlation function,[42–44]

$$G_{AA}=\left\langle A(0)A\left(t+\frac{i\beta\hbar}{2}\right)\right\rangle =\frac{1}{Z}\mathrm{Tr}(Ae^{iH(t+(i\beta\hbar/2)/\hbar}Ae^{-iH(t-(i\beta\hbar/2)/\hbar}), \tag{3}$$

which is obtained by shifting the domain of the quantum time correlation function from the real time axis by $-i\beta\hbar/2$. As the correlations are now measured between points in the complex time plane, $G(t)$ is also known as the complex time correlation function.[45] Introducing a complex time $\tau_c=t-i\beta\hbar/2$, one can write the symmetrized correlation function in position representation as

$$G_{AA}(t)=\frac{1}{Z}\int dxdx'A(x)A(x')\langle x'|e^{-iH\tau_c/\hbar}|x\rangle \times\langle x|e^{iH\tau_c^*/\hbar}|x'\rangle. \tag{4}$$

The propagation forward and backward along the real time axis, followed by that along the imaginary time axis (the Kadanoff–Baym contour)[46] present in $C(t)$ has now been replaced by the propagation along a contour in the complex time plane consisting of a forward propagation from x to x' by τ_c and backward propagation to x by τ_c^*. The difference between the two contours is illustrated in Fig. 1.

The complex time propagators can now be expressed as path integrals,

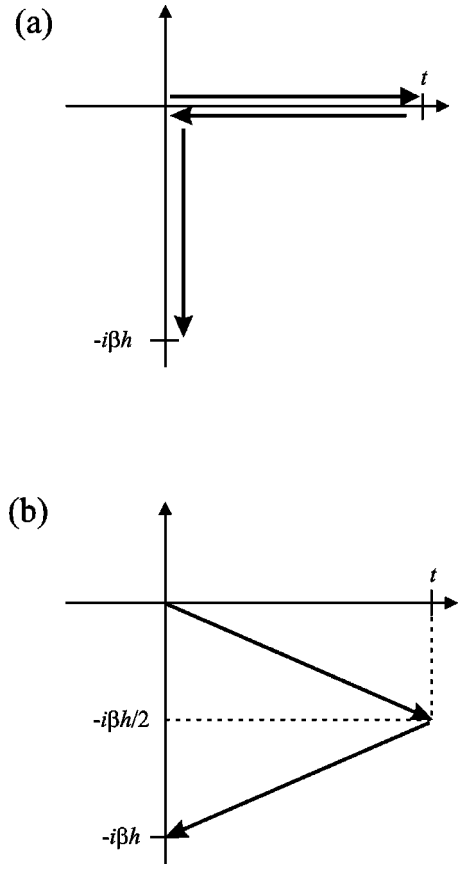

FIG. 1. A schematic representation of the propagation contour in the complex time plane. (a) is the Kadanoff–Baym contour arising in real-time quantum correlation functions and (b) is the propagation contour appearing in the symmetrized time correlation function. The arrows indicate the direction of propagation.

$$\langle x'|e^{-iH\tau_c/\hbar}|x\rangle = \int_x^{x'} Dx(z) e^{(i/\hbar)S[x(z);\tau_c]}, \tag{5}$$

with $S[x(z);\tau_c]$ being the classical action along the complex time path,

$$S[x(z);\tau_c] = \int_0^{\tau_c} dz \left[\frac{1}{2} m\dot{x}(z)^2 - V(x(z))\right]. \tag{6}$$

The principal advantage of the symmetrized time correlation functions is that in the path integral formulation, the complex time paths now do have a positive definite weight, and importance sampling techniques can be used to evaluate the necessary path integrals. Of course, the ''sign problem'' is still present since the complex phases have imaginary contributions. However, since the imaginary parts of the phase contributions for forward and backward complex time paths have opposite signs, the resulting cancellation should make the problem less severe, as was pointed out by Thirumalai and Berne.[42] Another advantage is that the forward and backward complex time contours form a cyclic path with equivalent weights, which allows efficient sampling methods such as staging[47] to be used to evaluate the integrals.

It should be also noted that, while the quantum time correlation function of Hermitian operators is a complex function of time, its symmetrized counterpart is a purely real, symmetric function. In addition, the transformation from $G(t)$ to $C(t)$ is nontrivial and involves further difficulties which will be addressed in a later section.

We conclude this section by considering the symmetrized time correlation function of a system bilinearly coupled to a harmonic dissipative environment. This important model[48] has been used extensively to study processes in condensed phase. The model allows the Hamiltonian to be split as follows:

$$H = H_S(p,x) + H_E(p_\alpha, x_\alpha) + H_I(x, x_\alpha), \tag{7}$$

where (p,x) represent the system coordinates and (p_α, x_α) are the harmonic degrees of freedom describing the environment. The path integrals over the latter can be performed analytically, and the propagator matrix elements in Eq. (4) are expressed as integrals over the system paths only, whereas the effects of the environment are contained in the Feynman–Vernon influence functional.[49] The influence functional gives rise to interactions that are nonlocal in time and involve couplings between different points along the complex time contour. For a harmonic environment, which is characterized by a spectral density $J(\omega)$, the symmetrized correlation function is given by

$$G_{AA}(t) = \frac{1}{Z}\int dx dx' A(x')A(x') \int_x^{x'} Dx(z) \times \int_{x'}^{x} Dx'(z) e^{(i/\hbar)\{S[x(z);\tau_c] - S[x(z);\tau_c^*]\}} I[x(z)], \tag{8}$$

where the influence functional $I[x(z)]$ is a functional of the complex time path given by[50]

$$I[x(z)] = \exp\left\{-\frac{1}{\hbar}\int dz \int_{z>z'} dz' x(z) L(z-z') x(z')\right\}, \tag{9}$$

with the integrations over complex time z evaluated along the contour in Fig. 1(b). $L(z-z')$ is the force autocorrelation function of the environment,

$$L(z-z') = \frac{1}{\pi}\int_0^\infty d\omega J(\omega) \frac{\cosh\left[\frac{\beta\hbar\omega}{2} - i\omega(z-z')\right]}{\sinh\left(\frac{\beta\hbar\omega}{2}\right)}. \tag{10}$$

III. PIMC SIMULATIONS

For the purpose of computer simulations, each of the complex time propagators in Eq. (4) is expressed as a product of P short time propagators over $\epsilon = \tau_c/P = \epsilon_r + i\epsilon_i$. Inserting complete sets of states gives

$$G_{AA}(t) = \frac{1}{Z}\int dx_1 \cdots dx_{2P} A(x_1)A(x_{P+1}) \times \langle x_{P+1}|e^{-iH\epsilon/\hbar}|x_P\rangle \cdots \langle x_2|e^{-iH\epsilon/\hbar}|x_1\rangle \times \langle x_1|e^{iH\epsilon^*/\hbar}|x_{2P}\rangle \cdots \langle x_{P+2}|e^{iH\epsilon^*/\hbar}|x_{P+1}\rangle. \tag{11}$$

A. Standard position basis representation of path integrals

Most of the simulations in this work were performed using the symmetric Trotter[51] splitting, with the short time approximation for the free particle propagator as shown in Eq. (12),

$$\langle x_{j+1}|e^{-iH\epsilon/\hbar}|x_j\rangle \approx \sqrt{\frac{m}{2\pi i\hbar\epsilon}}\exp\left\{\frac{i}{\hbar}\frac{m}{2\epsilon}(x_{j+1}-x_j)^2 - \frac{i}{\hbar}\epsilon\left(\frac{V(x_{j+1})+V(x_j)}{2}\right)\right\}. \tag{12}$$

Inserting this into Eq. (11) the expression for $G(t)$ becomes

$$G_{AA}(t)=\frac{1}{Z}\int dx_1\cdots dx_{2P}\,A(x_1)\times A(x_{P+1})\rho(x_1,\ldots,x_{2P};\epsilon)e^{i\phi(x_1,\ldots,x_{2P};\epsilon)}, \tag{13}$$

with the partition function given by

$$Z=\int dx_1\cdots dx_{2P}\,\rho(x_1,\ldots,x_{2P};\epsilon)e^{i\phi(x_1,\ldots,x_{2P};\epsilon)}. \tag{14}$$

$\rho(x_1,\ldots,x_{2P};\epsilon)$ is a positive definite function of the path given by

$$\rho(x_1,\ldots,x_{2P};\epsilon)=\left(\frac{m}{2\pi|\epsilon|^2}\right)^P\exp\left\{\frac{m\epsilon_i}{2|\epsilon|^2\hbar}\sum_{j=1}^{2P}(x_{j+1}-x_j)^2+\frac{\epsilon_i}{\hbar}\sum_{j=1}^{2P}V(x_j)\right\}, \tag{15}$$

while the phase information is contained in $\phi(x_1,\ldots,x_{2P};\epsilon)$,

$$\phi(x_1,\ldots,x_{2P};\epsilon)=\left(\frac{m\epsilon_r}{2|\epsilon|^2\hbar}\right)\left[\sum_{j=1}^{P}(x_{j+1}-x_j)^2-\sum_{j=P+1}^{2P}(x_{j+1}-x_j)^2\right] - \frac{\epsilon_r}{\hbar}\left[\sum_{j=2}^{P}V(x_j)-\sum_{j=P+2}^{2P}V(x_j)\right]. \tag{16}$$

Since it is positive definite, $\rho(x_1,\ldots,x_{2P};\epsilon)$ can be used as a weight in importance sampling. For this purpose, $G(t)$ is expressed in terms of averages over ρ as

$$G_{AA}(t)=\frac{\langle A(x_1)A(x_{P+1})e^{i\phi}\rangle_\rho}{\langle e^{i\phi}\rangle_\rho}, \tag{17}$$

where for a function of the path f the average over ρ is understood to be

$$\langle f\rangle_\rho=\frac{\int dx_1\cdots dx_{2P}f(x_1,\ldots,x_{2P})\rho(x_1,\ldots,x_{2P};\epsilon)}{\int dx_1\cdots dx_{2P}\rho(x_1,\ldots,x_{2P};\epsilon)}. \tag{18}$$

The two averages in Eq. (17) were evaluated using the staging PIMC algorithm.[47] For some of our model systems, notably the one-dimensional cases, weighted histogram analysis method[52] (WHAM) and umbrella sampling[53] from the zero-time distribution were used to optimize the averaging over configurations. This method has been used before[54] in the context of symmetrized time correlation functions, and details are available therein.

For the models involving systems coupled to a dissipative environment, the influence functional was discretized as

$$I(x_1,\ldots,x_{2P})=\exp\left\{-\frac{1}{\hbar}\sum_{j=1}^{2P}\sum_{k=1}^{j}x_j\alpha_{jk}x_k\right\}, \tag{19}$$

where the coefficients α_{jk} are given by

$$\alpha_{jk}=\begin{cases}\Delta_jL(z_j-z_k)\Delta_k, & j\neq k,\\ \frac{1}{2}\Delta_jL(z_j-z_k)\Delta_k, & j=k,\end{cases} \tag{20}$$

with the time step Δ_j determined by

$$\Delta_j=\begin{cases}i\epsilon_i, & j=1,P+1,\\ \epsilon, & 2\leqslant j\leqslant P,\\ -\epsilon^*, & P+2\leqslant j\leqslant 2P.\end{cases} \tag{21}$$

The same Trotter factorization was used in the imaginary time correlation functions in position basis representation, where the discretized expression for these is obtained by setting the real part of ϵ in Eqs. (15) and (16) to zero. In this case, the phase factor ϕ vanishes, and the expression becomes

$$C^i_{AA}(|j-k|\epsilon_i)=\frac{\int dx_1\cdots dx_{2P}A(x_i)A(x_j)\rho(x_1,\ldots,x_{2P};\epsilon_i)}{\int dx_1\cdots dx_{2P}\rho(x_1,\ldots,x_{2P};\epsilon_i)}, \tag{22}$$

which is then evaluated through staging PIMC simulations.

B. Discretized variable representation of path integrals

It is often advantageous to use the discrete variable representation (DVR) in the path integration which provides substantial reduction in the configuration space. The original coordinate representation can be recovered, if desired, by means of the one-dimensional DVR transformation,

$$|x'\rangle=\sum_{n=1}^{M}b_n|u_n\rangle,$$
$$b_n=\langle u_n|x'\rangle=\sum_{n'=1}^{M}\langle u_n|\Phi_{n'}\rangle\langle\Phi_{n'}|u_n\rangle, \tag{23}$$
$$\langle u_n|x|u_{n'}\rangle=\tilde{x}_n\delta_{n,n'},$$

where $\{u_n;\tilde{x}_n,n=1,\ldots,M\}$ are DVR eigenstates and eigenvalues, respectively, obtained from diagonalizing the position matrix of the M lowest eigenstates, $\{\Phi_n;E_n,n=1,\ldots,M\}$. The discretized path integral expression of the symmetrized correlation function, Eq. (11), for the system coupled to a harmonic environment takes the form

$$G_{AA}(t)=\frac{1}{Z}\sum_{k_0}^{M}\cdots\sum_{k_{2P+1}}^{M}\delta_{0,2P+1}\delta_{P,P+1}A(\tilde{x}_0)A(\tilde{x}_P)\times\prod_{j=P+1}^{2P}\langle u_{k_{j+1}}|e^{iH_S\epsilon^*/\hbar}|u_{k_j}\rangle\times\prod_{j=1}^{P}\langle u_{k_j}|e^{-iH_S\epsilon/\hbar}|u_{k_{j-1}}\rangle I(\tilde{x}_0,\ldots,\tilde{x}_{2P+1};\epsilon) \tag{24}$$

resulting from symmetric Trotter splitting of the total Hamiltonian[55] into a system dependent and system independent parts, which allows larger time step ϵ, i.e., a smaller P, than the standard Trotter split. Also, larger time steps can be used in quasiadiabatic path integration[19] (QUAPI) in which a counterterm corrected reference system potential is used. In addition to tremendous reduction of configuration space, a system-specific DVR also has the benefit of calculating the short-time system propagator in an exact manner such that,

$$\langle u|e^{-iH_S\epsilon/\hbar}|u'\rangle=\sum_{n=1}^{M}e^{-iE_n\epsilon/\hbar}\langle u|\Phi_n\rangle\langle\Phi_n|u'\rangle. \tag{25}$$

More accurate expressions for discretized influence functional coefficients and further details of this method can be found elsewhere.[55]

While for some cases full discretized space integration is possible, most problems still require the stochastic sampling method. For Monte Carlo importance sampling, analytic expression for the sampling function and phase of Eqs. (15) and (16), however, are no longer available in the discretized formalism. In this study, we used the absolute value of complex integrand without the operators as the sampling function,

$$\rho(\tilde{x}_0,\ldots,\tilde{x}_{2P+1};\epsilon)=\left|\delta_{0,2P+1}\delta_{P,P+1}\prod_{j=P+1}^{2P}\langle u_{k_{j+1}}|e^{iH_s\epsilon^*/\hbar}|u_{k_j}\rangle\times\prod_{j=1}^{P}\langle u_{k_j}|e^{-iH_s\epsilon/\hbar}|u_{k_{j-1}}\rangle I(\tilde{x}_0,\ldots,\tilde{x}_{2P+1};\epsilon)\right|. \tag{26}$$

IV. ANALYTIC CONTINUATION PROBLEM

The real-time, symmetrized, and imaginary time forms of the quantum time correlation function are related to each other via analytic continuations in the complex time plane.[56] Of these, the real-time quantum correlation function is the one directly related to the physically measurable dynamical quantities, and obtaining it is the primary goal of this work. To establish the relationship to the other forms it is useful to introduce the power spectrum, $I(\omega)$, which is a Fourier transform of the real-time correlation function

$$C(t)=\frac{1}{2\pi}\int_{-\infty}^{\infty}d\omega\, e^{i\omega t}I(\omega). \tag{27}$$

If one performs an analytic continuation to the imaginary time axis by letting $t\rightarrow i\tau$, one obtains the imaginary time correlation function which is a two-sided Laplace transform of the power spectrum

$$C^i(\tau)=\int_{-\infty}^{\infty}d\omega\, e^{-\omega\tau}I(\omega). \tag{28}$$

In order to compute $C(t)$ from $C^i(\tau)$ it is necessary to obtain $I(\omega)$ by performing an inverse transform of Eq. (28). Typically, the value of $C(\tau)$ is available from computer simulations at several values of τ with finite statistical errors. In this case, the inverse transform must be performed numerically, which is a highly unstable operation. Inverse Laplace transformation of noisy data is an ill-posed problem due to the highly singular nature of the Laplace kernel. As a consequence, specialized methods need to be used in order to control the numerical instability.

Methods based on maximum entropy and singular value decomposition have been employed for this purpose for a range of systems, such as quantum lattice models,[57] and an excess electron solvated in water,[36] helium, and xenon.[35] More recently, vibrational relaxation[38] and quantum reaction rates[39] have been studied as well. In all the cases it was found that very accurate data for $C(\tau)$ are necessary in order to obtain satisfactory results. Even then, the real-time correlation functions were accurate over relatively short times, so the method was limited to cases in which quantum correlations decay on that time scale.

The primary obstacle limiting the usefulness of imaginary time correlation functions is that their domain is restricted to between 0 and $\beta\hbar$. Moreover, for most cases of physical interest, $C(\tau)$ is symmetric around $\tau=\beta\hbar/2$, so that all of the correlation information is actually contained between 0 and $\beta\hbar/2$. Hence the domain of $C(t)$, which spans the entire real-time axis has been compressed into a small finite interval on the imaginary time axis. It is precisely this fact that is responsible for the sensitivity of the the real-time correlation functions to small variations in their imaginary time counterparts. This causes the instability of the numerical analytic continuation. The problem becomes more severe at higher temperatures, when the imaginary time domain contracts drastically, vanishing completely in the classical limit.

One way to avoid this limitation is to use the symmetrized time correlation function. $G(t)$ is obtained by shifting the domain of $C(t)$ to a line in the complex plane through analytic continuation $t\rightarrow t+i\beta\hbar/2$. For Hermitian operators, $G(t)$ is real and symmetric in time, so the relationship to $I(\omega)$, and therefore $C(t)$ is given by

$$G(t)=\frac{1}{\pi}\int_0^{\infty}d\omega\cos(\omega t)e^{-\beta\hbar\omega/2}I(\omega). \tag{29}$$

Following the procedure used for imaginary time correlation functions, one can perform a numerical analytic continuation to obtain $C(t)$ by inverting Eq. (29). The integration kernel is still ill-behaved but to a lesser degree than in Eq. (28). Hence, the resulting real-time correlation functions should be less sensitive to the statistical errors in simulation data for

$G(t)$. The reason for this is that the domain of $G(t)$ is not restricted to an interval, but extends over all values of real time t, and the temperature affects only the imaginary time component of the complex time argument, or the degree of displacement from the real-time axis. Thus, in a sense the complex time correlations contained in $G(t)$ represent a compromise between conditions favorable to simulation, and those favorable to the analytic continuation:

(1) The presence of the real time component extends the domain, thereby reducing the numerical instability of the analytic continuation; nonetheless it introduces oscillating phase factors into the path integrals.
(2) The imaginary time component allows importance sampling to be used to evaluate the oscillatory integrals present in $G(t)$; however the presence of the imaginary time component is the cause of the numerical instability in the inversion.

Hence, it is plausible to expect that by applying the ME numerical analytic continuation method to the symmetrized time correlation data, or perhaps in combination with imaginary time data, one will be able to compute real-time quantum correlation functions for longer times.

V. MAXIMUM ENTROPY METHOD

The maximum entropy[58,59] (ME) inversion method has been shown to be useful for many problems in which there is incomplete and noisy data. The method itself requires only the knowledge of the transformation which relates the data and the solution. Furthermore, prior knowledge about the solution is included in a logically consistent fashion. As such, ME is ideally suited for solving ill-posed mathematical problems. A particularly important class of such problems involves inverting integral equations of the type,

$$D(\tau)=\int d\omega K(\tau,\omega)A(\omega), \tag{30}$$

where $K(\tau,\omega)$ is a singular kernel. Equations (27) and (28) which relate the real-time and imaginary time correlation functions with the power spectrum belong to this class. If the data set $D(\tau)$ is noisy and incomplete, the solution $A(\omega)$, also referred to as the map, cannot be determined uniquely. Maximum entropy criteria provide a method for determining the most probable inversion consistent with the data. This method is based on Bayesian inference. Typically, the data are known only at a discrete set of points $\{\tau_i\}$, and we likewise seek a solution at a discrete set of points $\{\omega_j\}$. The maximum entropy method selects a solution which maximizes the probability of the map $\mathbf{A}$ given a data set $\mathbf{D}$, known as the posterior probability,[57,58]

$$\mathcal{P}(\mathbf{A}|\mathbf{D})\propto\exp(\alpha S-\chi^2/2)=e^{Q}. \tag{31}$$

Here χ^2 is the standard mean squared deviation from the data

$$\chi^2=\sum_{j,k}\left(D_j-\sum_l K_{jl}A_l\right)[C^{-1}]_{jk}\left(D_k-\sum_l K_{kl}A_l\right), \tag{32}$$

where C_{jk} is the covariance matrix,

$$C_{jk}=\frac{1}{M(M-1)}\sum_{l=1}^{M}(\langle D_j\rangle-D_j^{(l)})(\langle D_k\rangle-D_k^{(l)}), \tag{33}$$

with M being the number of measurements.

S is the information entropy, the form of which is axiomatically chosen to be

$$S=\sum_k \Delta\omega\left(A_k-m_k-A_k\ln\frac{A_k}{m_k}\right). \tag{34}$$

In this formulation the entropy is measured relative to a default model $m(\omega)$ which can contain prior information about the solution and α is a positive regularization parameter.

Finding a map $\mathbf{A}$ which maximizes the posterior probability is a maximization problem in N variables, where N is the number of points $\{\omega_k\}$ at which the solution is evaluated. The solution obtained in this way is still conditional on the arbitrary parameter α, which can be interpreted as a regularization parameter controlling the smoothness of the map. Large values of α lead to a result primarily determined by the entropy function and hence the default model. Small α in turn lead to a map determined mostly by the χ^2 and thus to a closer fitting of the data. The principal drawback is that, along with the data, the errors would be fit as well.

In this study α is obtained according to the L-curve method.[60,61] The value of α is selected by constructing a plot of $\log[-S(\mathbf{A})]$ vs $\log\chi^2$. This curve has a characteristic L-shape, and the corner of the L, or the point of maximum curvature, corresponds to the value of α which is the best compromise between fitting the data and obtaining a smooth solution.

We employ a maximization algorithm due to Bryan,[62] which reduces the space in which the search for the solution is performed. The kernel is first factored using singular value decomposition $K=V\Sigma U^T$. The singular nature of the kernel ensures only a small number of eigenvalues of Σ will be nonsingular. Since the space spanned by the rows of K is the same as that spanned by the columns of U associated with nonsingular eigenvalues, the search for the solution can be performed in this singular space of dimensionality N_s, where N_s is the number of nonsingular eigenvalues. The solution in singular space is expressed in terms of the vector $\mathbf{u}$, which is related to the N dimensional map space via

$$A_j=m_j\exp\left(\sum_{l=1}^{N_s}U_{jl}u_l\right). \tag{35}$$

This exponential transformation is useful since it ensures the positivity of the solution.

In this study we use a flat default map, which satisfies a known sum rule, such as the integral over $A(\omega)$. Other choices of $m(\omega)$ and their effect on the quality of the results will be the subject of future investigation.

One should note that the important precondition to the successful application of the ME method is that the data be Gaussian distributed and independent. Thus care must be taken to ensure that the simulation data satisfies these conditions as closely as possible. Ideally, there should be no correlation between different data points. If the simulation

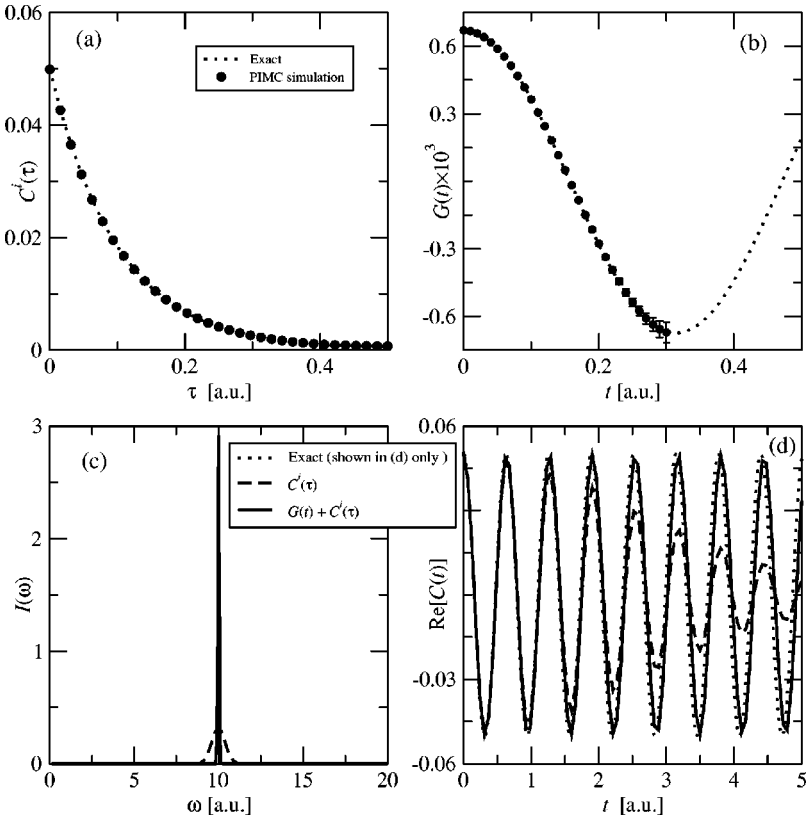

FIG. 2. Analytic continuation results for the linear harmonic oscillator of frequency $\omega_0=10.0$ a.u. at the inverse temperature $\beta=1.0$ a.u. In (a) we show the imaginary time correlation function computed by PIMC simulation (circles) compared to the exact result (dotted line). In (b) we show the same for the symmetrized time correlation function, computed by PIMC up to $t=0.3$ a.u. In (c) we show the power spectra obtained by ME continuation of imaginary time data (broken line) and a combination of symmetrized and imaginary time data (solid line). In (d) we show the real parts of the corresponding real-time correlation functions compared to the exact result (dotted line).

method does introduce correlation, the nature and the extent of the correlations needs to be expressed in terms of the covariance matrix.

VI. RESULTS FOR SEVERAL BOUND QUANTUM SYSTEMS

The approach described in the previous section was tested by computing quantum time correlation functions for several bound systems. In all cases, we computed the position autocorrelation functions, that is we take $A(x)=x$ in Eq. (2). These are directly related to absorption spectra in the dipole limit, with the photon absorption cross section given by

$$\sigma(\omega)=\left(\frac{4\pi}{\hbar c}\right)\omega(1-e^{-\beta\hbar\omega})I(\omega), \tag{36}$$

where $I(\omega)$ is given by Eq. (27). In most cases, we used the standard position basis representation, with the Trotter split of the short time propagator shown in Eq. (12) to discretize the path integrals required to compute the symmetrized time correlation functions $G(t)$ and the corresponding imaginary time correlation functions $C^i(\tau)$. This approach was chosen to keep the method computationally simple, applicable to a wide variety of systems, and to avoid using any *a priori* approximations. In a few cases we computed $G(t)$ using a more advanced approximation to the propagators, based on QUAPI with DVR expansion.

The simulations were performed using the staging PIMC method. The correlation function data was block-averaged to remove the correlations between successive Monte Carlo steps, and the length of blocks was adjusted to ensure the Gaussian distribution of the data. This was checked by computing the skewness and the kurtosis of the block averages for each imaginary time data point $\{\tau_i\}$. In all cases it was found that the data are within the norm of a Gaussian distribution. The corresponding covariance matrix was computed from the block averages using Eq. (33).

For imaginary time correlation functions, the data for all values of imaginary time are obtained from a single simulation. This introduced strong correlations between data for different imaginary times. Hence, large numbers of blocks were required to accurately evaluate the off-diagonal covariance matrix elements. This was necessary since strong correlations between data lead to an unstable spectral analysis of the covariance matrix with eigenvalues spanning several orders of magnitude. On the other hand, symmetrized time correlation functions were computed by performing a separate simulation for each value of real time. As a result, there are no correlations between data points corresponding to different times, the covariance matrix is diagonal, and smaller numbers of blocks were required. Such data is therefore more suitable for ME inversion.

A. One-dimensional systems

We first tested the method on two nondissipative one-dimensional bound systems. In both of these cases the spectral densities of the quantum position autocorrelation functions consist of discrete lines corresponding to various quantum transitions, and as a consequence, the correlation functions will not dephase, but will oscillate indefinitely. The exact results were computed by matrix diagonalization of the corresponding Hamiltonians.

The first system considered is a linear harmonic oscillator of frequency $\omega_0 = 10$ a.u. at the inverse temperature $\beta = 1.0$ a.u. In Figs. 2(a) and 2(b) we show the imaginary time and symmetrized correlation functions computed by PIMC simulations. The imaginary time path integrals were discretized into $P = 64$ slices, and a total of 2×10^6 configurations were generated, which were divided into 200 blocks. For $G(t)$, the complex time paths were discretized into $P = 32$ slices per path, and the averages were obtained from 25×10^7 configurations by umbrella sampling from the zero-time distribution to increase the efficiency of the averaging and reduce statistical errors due to phase oscillations. The data was computed at intervals of $\Delta t = 0.01$ a.u. up to $t = 0.3$ a.u.

Figure 2(c) shows the power spectra obtained by ME analytic continuation of the imaginary time data, and the simultaneous analytic continuation using both the imaginary time and symmetrized time correlation functions. The real parts of the corresponding real-time correlation functions are shown in Fig. 2(d) in comparison with the exact results. The continuation of the combination of imaginary and symmetrized time correlation data leads to a significant improvement over using imaginary time data alone. In particular, the spectral line at $\omega = \omega_0$ is significantly narrowed, leading to a longer decoherence time. As a consequence, correct coherence behavior is retained for more than eight oscillation periods, while imaginary time results decohere significantly after three periods.

We next examined an anharmonic system, namely a one-dimensional quartic oscillator, given by the Hamiltonian

$$H = \frac{p^2}{2m} + ax^4. \tag{37}$$

The calculations were performed for $m = 1836.15$ a.u. (corresponding to the mass of a proton) and $a = 0.001\,194$ a.u. at the temperature of 200 K ($\beta = 1578.78$ a.u.). In this regime, the dynamics are dominated by the two-state $|1\rangle \rightarrow |2\rangle$ transition, with a small contribution from the $|1\rangle \rightarrow |3\rangle$ transition. The relative intensities are shown in Fig. 3(a). The imaginary time path integral was discretized into $P = 64$ slices, and a total of 10^6 configurations were generated, which were divided into 100 blocks. The symmetrized time correlation function was calculated from a total 10^6 configurations, with 2×10^6 configurations sampled from each of the respective distributions at $t/\beta\hbar = 0, 0.1, 0.2, 0.3$ and 0.4, which were stored on disk. WHAM was then used to extract averages from these configurations in the effort to improve the averaging and reduce statistical error. The values of $G(t)$ were computed at intervals of $\Delta t = 15.8$ a.u. up to $t = 710.5$ a.u.

As in the case of the harmonic oscillator, ME inversion was performed using imaginary time data alone, and using a combination of short time symmetrized and imaginary time correlation data. The resulting power spectra and the real parts of the corresponding time correlation functions are shown along with the exact results in Figs. 3(a) and 3(b). Once again, the use of $G(t)$ improves the results, giving a better reproduction of the principal transition. The correlation function thus obtained is very accurate over five periods,

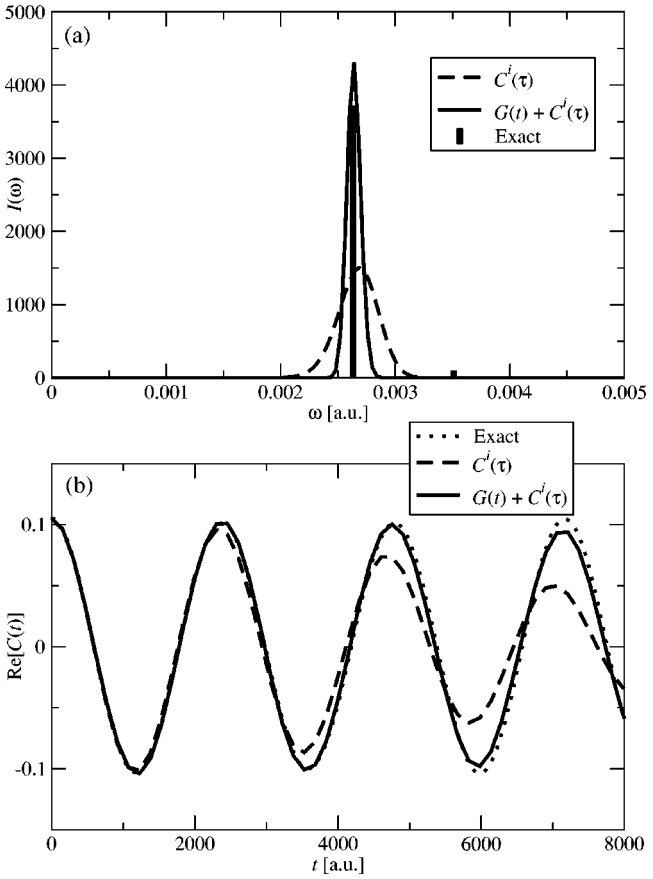

FIG. 3. Analytic continuation results for the quartic oscillator potential at the temperature of 200 K. In (a) we show the power spectra of the position correlation functions computed by ME analytic continuation of imaginary time data (broken line) and the combination of imaginary and symmetrized time correlation data (solid line). The solid bars show relative intensities of the two principal transition lines active at this temperature. In (b) we show the real parts of the corresponding real-time correlation functions in comparison with the exact result (dotted line).

or more than $t = 8000$ a.u. In comparison, the result based solely on imaginary time data starts dephasing already at $t = 3000$ a.u. However, neither result is able to capture the effect of the small contribution from the second transition.

In both one-dimensional systems examined, the ME analytic continuation was able to extract accurate real-time correlation functions for time intervals up to ten times longer than the range of the symmetrized time correlation data supplied from the simulation. Although these results are very encouraging, it should be noted that both of these systems are dominated by a single frequency. It should be noted that the contributions from the higher state transitions become more important at high temperatures. However, real-time path integrals in the standard position basis representation are much harder to converge in these cases due to higher frequency oscillations of the integrands, and hence can be evaluated only for very short times without incurring prohibitive computational costs. Thus, it would be difficult to obtain the data at the sufficiently long times required for the resolution of the discrete spectral lines through analytic continuation. Similarly, the imaginary time correlation functions are harder to compute at higher temperatures due to the increased stiffness of the harmonic bonds. Moreover, the ME

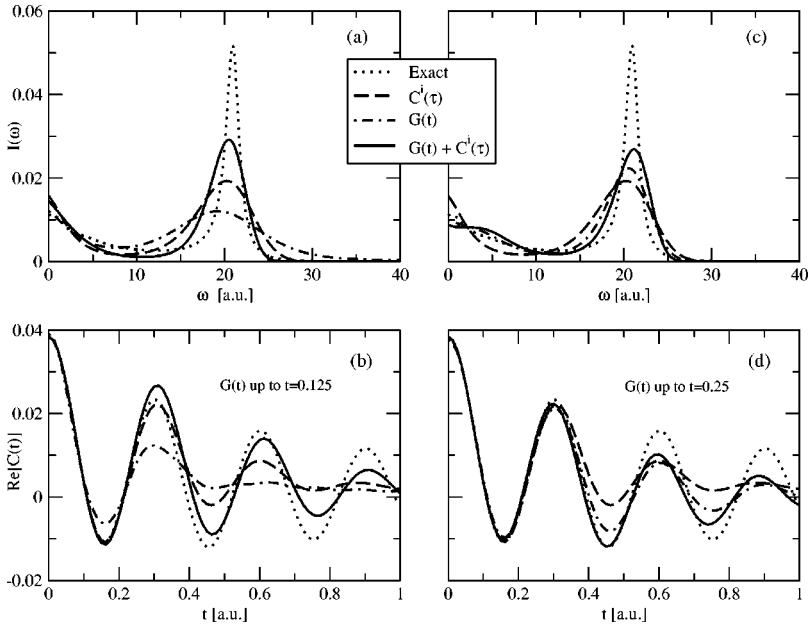

FIG. 4. Analytic continuation results for a harmonic oscillator coupled to a harmonic environment. In (a) we show the power spectra and in (b) the real parts of the corresponding real-time position correlation functions obtained by ME continuation of imaginary time data (broken line), symmetrized time correlation data (dotted–dashed line) and the combination of the two (solid line) in comparison with the exact result (dotted line). The symmetrized time correlation function data was included up to $t=0.5$ a.u. In (c) and (d) we show the same results using symmetrized time correlation data up to $t=1.0$ a.u.

method was designed and shown to give best results for continuous smooth spectra,[38,40] which are the characteristic of most physical condensed phase systems. In the next two subsections we test the method for systems that are coupled to a dissipative environment in which the dynamics is characterized by a broad range of frequencies.

B. Harmonic oscillator coupled to harmonic environment

In addition to being a classic model for vibrational relaxation processes, this is the only many body system for which exact solutions for quantum position autocorrelation functions are available. In particular, it was shown that the classical photon absorption cross section, obtained in closed form by solving the generalized Langevin equation[63] is equal to the quantum one.[64] As such, this system was subject to investigation using ME analytic continuation methods previously.[38] The total Hamiltonian is given by

$$H=\frac{p^2}{2m}+\frac{1}{2}m\omega_0^2x^2+\sum_\alpha\left(\frac{p_\alpha^2}{2m_\alpha}+\frac{1}{2}m_\alpha\omega_\alpha^2x_\alpha^2\right)-x\sum_\alpha c_\alpha x_\alpha, \quad (38)$$

where (x,p) correspond to the system, in this case the harmonic oscillator and (x_α,p_α) correspond to a harmonic mode of the environment with mass m_α and frequency ω_α. We use the influence functional approach and express the properties of the environment in terms of the spectral density function $J(\omega)$,

$$J(\omega)=\frac{\pi}{2}\sum_\alpha\frac{c_\alpha^2}{m_\alpha\omega_\alpha}\delta(\omega-\omega_\alpha), \quad (39)$$

which was computed from the classical friction kernel $\zeta(t)$,

$$J(\omega)=\omega\int_0^\infty dt\cos(\omega t)\zeta(t). \quad (40)$$

The analytic form of the friction kernel was chosen to fit simulation data for a fluid of Lennard-Jones particles, and is given by[38]

$$\zeta(t)=\zeta_0\{e^{-\alpha_1(ft)^2}[1+a_1(ft)^4]+a_2(ft)^4e^{-\alpha_2(ft)^2}\}. \quad (41)$$

The particular parameters chosen are $\zeta_0=225$, $a_1=1.486\times10^5$, $a_2=285$, $\alpha_1=903$ and $\alpha_2=75.0$. In this study we consider the case of low damping ($f=0.2$) at the inverse temperature $\beta=0.25$ a.u. The bare oscillator frequency ω_0 was chosen to be 20 a.u. Under these conditions, the system couples weakly to the environment, and exhibits complex relaxation dynamics, which is evident from the line shape of the power spectrum of the position autocorrelation function shown in Figs. 4(a) and 4(c). Two principal features are a sharp peak at the oscillator frequency, and a broad low intensity phonon band extending over the entire low frequency region. As a result, the system exhibits a long relaxation time and the correlation functions were difficult to obtain by ME analytic continuation of imaginary time data alone.[38] Therefore, it is an appropriate test for the new approach.

The influence functional coefficients were computed from $J(\omega)$ using Eq. (10) and Eq. (20). The PIMC simulations were then performed to evaluate the path integrals in Eq. (8) as well as the ones arising in corresponding imaginary time correlation function expression. The imaginary time path integral was discretized with $P=128$ time slices, and the correlation function was computed from a total of 2×10^7 configurations divided into 200 blocks. The symmetrized correlation function was computed at intervals of $\Delta t=0.005$ a.u. up to a total time of $t=0.25$ a.u. (corresponding to $\beta\hbar$). A separate simulation was performed for each value of t, and the numbers of configurations ranged from 10^8 to 2×10^8 for the longest times. The complex paths were discretized with $P=8$ slices each (for a total of 16 time slices) in each simulation.

Two sets of data were used as input for ME inversion. In the first case, symmetrized time correlation data was in-

cluded up to $t=0.125$ a.u., which is the same as the imaginary time range. The ME inversions were performed using imaginary time data alone, symmetrized time correlation function alone and the combination of the two. The results for power spectra and the real parts of the corresponding position autocorrelation functions are shown in Figs. 4(a) and 4(b) in comparison with exact results. The same procedure was then performed using $G(t)$ data for up to $t=0.25$ a.u., or twice the range of the first case, with the results shown in Figs. 4(c) and 4(d).

In both cases, including symmetrized time correlation function data leads to an improvement. The continuation using imaginary time data results in a real-time correlation function accurate to $t=0.3$ a.u., or on the order of $\beta\hbar$. This is superior to the results using only $G(t)$ data in the first case (i.e., data up to $t=0.125$ a.u.), but in the second case, continuation using longer time symmetrized correlation function data (up to $t=0.25$ a.u.) yields a real-time correlation function accurate to $t=0.45$ a.u. In particular, the low frequency portion of the spectrum is well reconstructed. This behavior is not unexpected, as the power spectrum of $G(t)$ is related to $I(\omega)$ through $G(\omega)=e^{-\beta\hbar\omega/2}I(\omega)$, it is thus primarily determined by the low frequency region of $I(\omega)$.

The continuation using the combination of imaginary and symmetrized time correlation functions in both cases leads to improvement over that using the either data alone. In particular, major improvement is observed in the first case, where qualitative accuracy is observed up to $t=1.0$ a.u. In the second case, as longer time $G(t)$ is used, this data tends to dominate the ME inversion, and hence the results of continuation of the combined data are similar, although somewhat better than using $G(t)$ alone. In general, using symmetrized correlation functions doubles the time interval over which the analytically continued correlation functions are accurate, and results in qualitative accuracy over much longer times.

It should be noted, that in order to reduce the statistical errors (which increases rapidly with the number of integration variables) in PIMC simulations of $G(t)$, a relatively small number of time slices was used, which introduced some discretization error. Thus a part of the error in real-time correlation functions (particularly the slight shift of the principal peak in the power spectrum) can be attributed to this fact. This part of the error is systematic and will decrease if the Trotter number is increased.

C. Quartic oscillator coupled to harmonic environment

We next examine a highly anharmonic system, namely a quartic oscillator interacting with a dissipative environment. The Hamiltonian is given by

$$H=\frac{p^2}{2m}+ax^4+\sum_\alpha\left(\frac{p_\alpha^2}{2m_\alpha}+\frac{1}{2}m_\alpha\omega_\alpha^2x_\alpha^2\right)-x\sum_\alpha c_\alpha x_\alpha, \tag{42}$$

with the system parameters same as those of a quartic oscillator described in a previous section. The environment is characterized by an Ohmic spectral density

$$J(\omega)=\eta\omega e^{-\omega/\omega_c}, \tag{43}$$

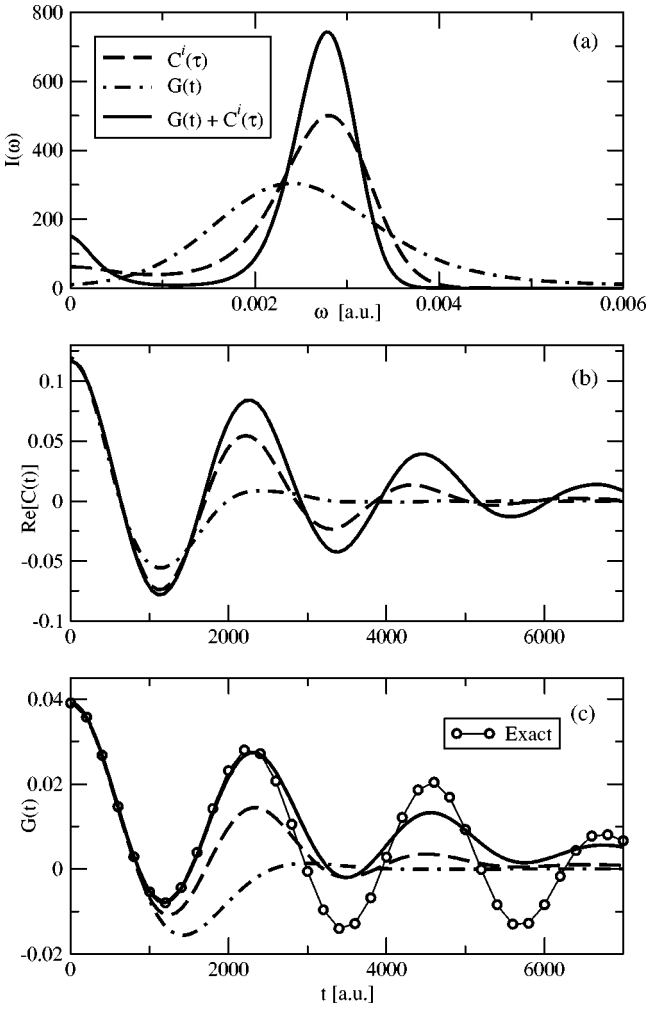

FIG. 5. Analytic continuation results for a quartic oscillator coupled to a harmonic environment at the temperature of 200 K. The symmetrized time correlation function data was included up to $t=790$ a.u. In (a) we show the power spectra and in (b) the real parts of the corresponding real-time position correlation functions computed by ME continuation of imaginary time data (broken line), symmetrized time correlation data (dotted–dashed line) and the combination of the two (solid line). In (c) we show the symmetrized correlation functions calculated from the power spectra in (a) in comparison with the exact result (empty circles).

with the cutoff frequency $\omega_c=4.556\times10^{-4}$ a.u., and the coupling strength $\eta=12.55$ a.u., which again leads to a relatively weak coupling with the system characterized by long relaxation times, and therefore a difficult regime for analytic continuation methods.

We have used two simulation approaches for this system. First an approach identical to the one used for the vibrational relaxation of the harmonic oscillator was implemented. The imaginary time path integral was discretized with $P=64$ time slices, and the corresponding correlation function computed from 10^7 PIMC configurations divided into 200 blocks. The symmetrized time correlation function was calculated at intervals $\Delta t=31.6$ a.u. $(0.02\,\beta\hbar)$ up to a maximum time of $t=1578.78$ a.u. $(\beta\hbar)$, using 5×10^7 configurations at short times and up to 8×10^8 configurations for the longest times. The complex time paths were discretized with $P=8$ slices for each of the two paths.

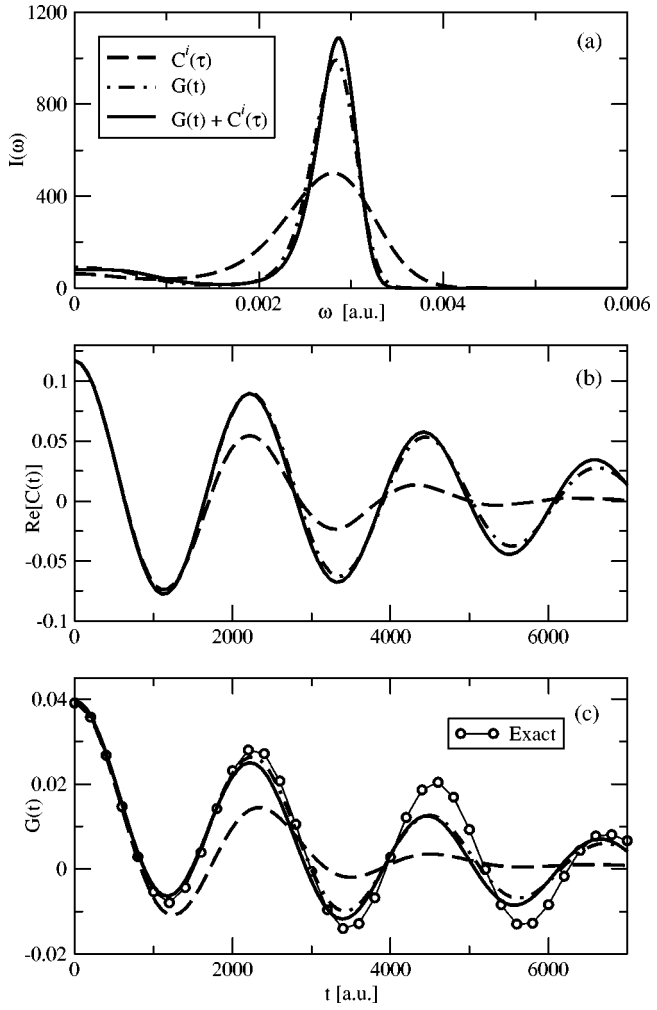

FIG. 6. Analytic continuation results for a quartic oscillator coupled to a harmonic environment at the temperature of 200 K. The symmetrized time correlation function data was included up to $t=1580$ a.u. In (a) we show the power spectra and in (b) the real parts of the corresponding real-time position correlation functions computed by ME continuation of imaginary time data (broken line), symmetrized time correlation data (dotted–dashed line) and the combination of the two (solid line). In (c) we show the symmetrized correlation functions calculated from the power spectra in (a) in comparison with the exact result (empty circles).

The ME analytic continuation was then performed as before using the two correlation functions and their combination. In the first case we used $G(t)$ data up to $t=790$ a.u. $(0.5\beta\hbar)$. The resulting power spectra are shown in Fig. 5(a) and the real parts of the corresponding real-time correlation functions in Fig. 5(b). Due to the presence of the anharmonic potential, the full dynamics cannot be obtained exactly. However, it is possible to compute the symmetrized correlation functions up to intermediate times (several multiples of $\beta\hbar$) using a nonstochastic approach based on exact evaluation of integrals in the discrete variable representation of path integrals in Eq. (24). These are shown in Fig. 5(c) in comparison with the symmetrized time correlation functions computed from the power spectra in Fig. 5(a) using Eq. (29). In the second case, the same procedure was performed while using longer time data for $G(t)$ as input, up to $t=1580$ a.u., which corresponds to $\beta\hbar$ and approaches the limit attainable with this simulation scheme. The results of analytic continuation, as well as the corresponding exact integration data for $G(t)$ are shown in Figs. 6(a), 6(b), and 6(c).

The results show a similar trend to the one observed in the case of the harmonic oscillator vibrational relaxation. The use of short time (up to a cutoff time of $t_c=790$ a.u.) $G(t)$ data together with imaginary time data leads to a considerable improvement over the inversion using imaginary time data alone, more than doubling the time interval over which the exact symmetrized correlation data is accurately reproduced, as can be seen in Fig. 5(c). Using only imaginary time data still gives better results than using only short time $G(t)$ data. However, as shown in Fig. 6, if longer time $G(t)$ data is used in the inversion, the result of a continuation using a combination of imaginary and symmetrized time correlation data is virtually identical to using the symmetrized time correlation data alone. Both show a major improvement, accurately reproducing exact $G(t)$ data up to $t=6000$ a.u., as can be seen in Fig. 6(c), which is almost fivefold longer than the range of accuracy of analytically continued imaginary time data.

This effect was observed in case of the harmonic oscillator as well, the reason behind it being that the inversion data is increasingly dominated by $G(t)$ as the domain of the symmetrized correlation data is extended, up to a point where the imaginary time data plays a negligible role. It is therefore interesting to observe whether a systematic improvement in accuracy of real-time correlation functions resulting from analytic continuation can be achieved by successively extending the domain of $G(t)$ used in ME inversion.

For this purpose we used a specialized DVR based PIMC method described in Sec. III. Although limited to systems in which the interaction with the environment can be expressed in terms of a quadratic influence functional, and thus less general then the standard approach used so far, this method allows integrals over continuous variables extending over all space to be reduced to a sum over a finite number of paths. In addition, quasiadiabatic modification[19] was applied to the path integrals which allowed fewer time slices to be used. Both of these serve the purpose of dramatically reducing the size of the space that must be stochastically sampled, which in turn results in fewer phase cancellations and a slower growth of statistical errors with time. Hence, using this method one is able to compute $G(t)$ for considerably longer times than $\beta\hbar$ which is more or less the limit attainable using the standard position basis discretization. This is particularly important in simulating systems at higher temperatures, as $\beta\hbar$ then corresponds to a very short time.

We have computed the symmetrized time correlation function for the dissipative quartic oscillator at two temperatures, 200 K, which was discussed above, and at 1000 K. For the latter it was very difficult to obtain converged results at sufficiently long times using the standard method. We have used MC importance sampling to evaluate the sums over paths in Eq. (24), using the sampling function given by Eq. (26). For the lower temperature case, 4 DVR states were used and the complex paths were discretized into 8 time

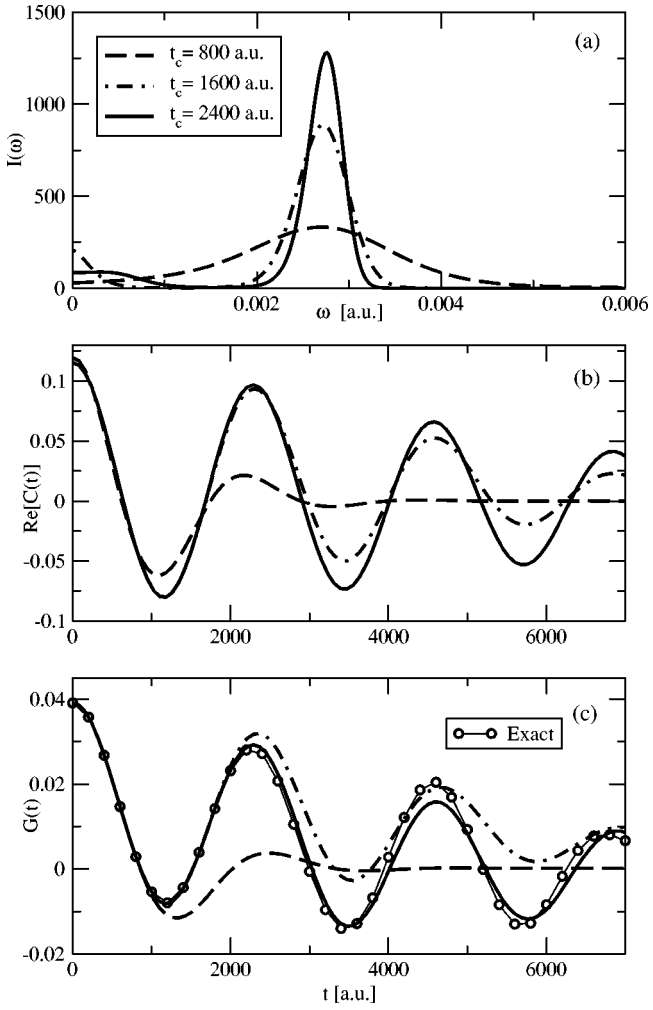

FIG. 7. Analytic continuation results for a quartic oscillator coupled to a harmonic environment at the temperature of 200 K. In (a) we show the power spectra and in (b) the real parts of the corresponding real-time position correlation functions computed by ME continuation of symmetrized time correlation function data computed by simulation up to the cutoff time $t_c=800$ a.u. (broken line), $t_c=1600$ a.u. (dotted–dashed line), and $t_c=2400$ a.u. (solid line). In (c) we show the symmetrized correlation functions calculated from the power spectra in (a) in comparison with the exact result (empty circles).

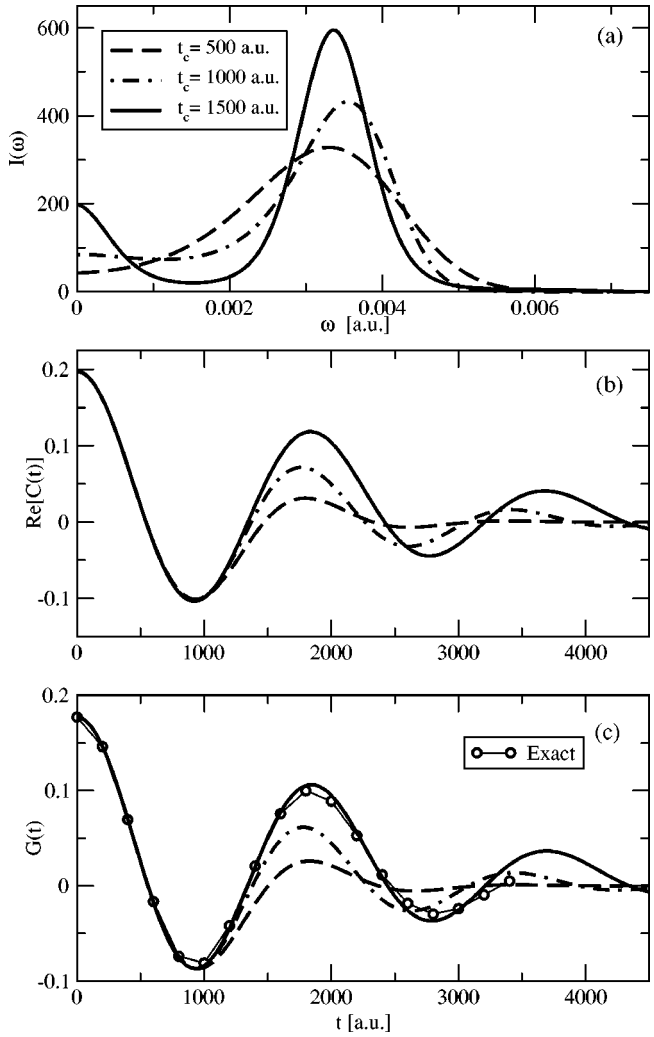

FIG. 8. Analytic continuation results for a quartic oscillator coupled to a harmonic environment at the temperature of 1000 K. In (a) we show the power spectra and in (b) the real parts of the corresponding real-time position correlation functions computed by ME continuation of symmetrized time correlation function data computed by simulation up to the cutoff time $t_c=500$ a.u. (broken line), $t_c=1000$ a.u. (dotted–dashed line), and $t_c=1500$ a.u. (solid line). In (c) we show the symmetrized correlation functions calculated from the power spectra in (a) in comparison with the exact result (empty circles).

slices par path, while for the higher temperature case we used 7 DVR states and 6 time slices par path.

With these parameters we were able to obtain converged results for $G(t)$ up to $t=3000$ a.u. for the low temperature case and $t=2000$ a.u. for the high temperature case. We used ME analytic continuation to compute the real-time correlation functions from symmetrized correlation functions, for several sets of $G(t)$ with increasing cutoff time t_c. The results for the power spectra, and the real-time and symmetrized time correlation functions computed from the former are shown in Figs. 7(a), 7(b), and 7(c), respectively, for the lower temperature case and Fig. 8 for the higher temperature one.

For both temperatures a systematic improvement can be observed as the time domain of the simulated $G(t)$ data is extended. This is evident in comparison with exact $G(t)$ results in Figs. 7(c) and 8(c), which are accurately reproduced as the cutoff time is increased. It should be noted that the gain in the time range [i.e., the range over which the analytically continued real-time results are accurate compared to the cutoff time up to which the $G(t)$ data are available] appears to increase with increasing cutoff time. As the computational effort for real-time path integrals increases exponentially with time, this is particularly significant, as it allows one to compute accurate quantum time correlation functions for significantly longer times than that could be attained by direct simulation.

VII. CONCLUSION

We have presented a new method for obtaining quantum time correlation functions through maximum entropy numerical analytic continuation using path integral Monte Carlo simulations. Previous approaches focused on using PIMC simulations to estimate dynamics in imaginary time. These data were then numerically inverted to obtain real-

time correlation functions. However, due to the highly singular nature of exponentially decaying inversion kernel, this operation is highly unstable. As a result, even small statistical errors in imaginary time data can lead to large deviations in analytically continued real-time correlation functions. The reason for this instability is that the correlation information, spanning the entire real-time axis, is compressed into an interval of $[0,\beta\hbar/2]$ in imaginary time. The problem becomes particularly severe at higher temperatures, for which the imaginary time domain further contracts.

In order to alleviate this problem we have introduced the symmetrized time correlation function, $G(t)$, the domain of which has been displaced from the real-time axis by $-i\beta\hbar/2$. Hence, the domain of this correlation function lies in the complex plane, with its real part spanning all values of time, and the imaginary part a constant. As a result, the symmetrized form is related to the real-time correlation function via an analytic continuation operation which is numerically more stable than in case of the imaginary time.

This benefit comes with a price, though, as the path integral that must be evaluated for the determination $G(t)$ contains oscillating phase factors due to complex time correlations. Nonetheless, in contrast to the real-time correlation functions, the complex time paths do have a positive definite weight, and PIMC methods can thus be directly used to compute $G(t)$. We have described several simulation methods based on position basis or DVR of the path integral that can be used to estimate the symmetrized time correlation functions. The symmetrized time correlation data was then used on its own or in combination with imaginary time data in a ME numerical analytic continuation procedure to compute the corresponding real-time correlation functions.

We have tested the method for two one-dimensional, nondissipative systems and two systems interacting with a dissipative environment. In all cases, using the combination of imaginary and symmetrized time correlation data in the analytic continuation process resulted in real-time correlation functions that were accurate over much longer times than those obtained from imaginary time data on its own. In particular, we observe that as the time domain (i.e., the cutoff time up to which simulation data is available) of the symmetrized time correlation data used in analytic continuation is lengthened, the range over which the real-time correlation functions are accurate increases substantially. Moreover, for longer time domains, the symmetrized time correlation data dominates in the ME inversion scheme, and combination with imaginary time data leads to the same result as using $G(t)$ data on its own. This clearly shows that expanding the time domain leads to a more stable inversion.

In contrast to analytic continuation utilizing only imaginary time correlation data, analytic continuation using the symmetrized time correlation function can be systematically improved by increasing the real-time cutoff. This is particularly evident in results for the quartic oscillator in Figs. 7 and 8, where using increasing values of the cutoff time for the $G(t)$ data leads to real-time correlation functions that are accurate over progressively longer times.

The main drawback of this approach is the difficulty of converging PIMC simulations for $G(t)$ at large values of time, due to strong phase cancellations. Hence, using the standard simulation method based on primitive discretization of path integrals in position basis representation one can reach times longer than $\beta\hbar$ only with difficulty, as exceedingly large numbers of Monte Carlo configurations need to be sampled. In particular, we note that that the rate of growth of statistical error with time correlates strongly with the size of the space (i.e., number of integration variables) that is sampled. In case of the primitive discretization, we observe that for Trotter numbers larger than $P=60$ it was difficult to obtain converged results for even short times. On the other hand, many quantum systems might require substantially higher Trotter numbers to represent the continuum adequately.

Thus it is of considerable interest to investigate better discretization schemes which allow smaller number of time slices to be used and lead to a reduction of the overall integration space. An example of such a scheme is the DVR with system specific propagators, described in Sec. III. Using this method it was possible to obtain converge results for $G(t)$ at much longer times, allowing more accurate reconstruction of real-time correlation functions. Generalizing this approach will be a subject of future study. In addition, we plan to use the methodology described in this work to study quantum reaction rates and transport coefficients.

ACKNOWLEDGMENT

This work was supported by a grant from the National Science Foundation.

[1] N. Metropolis, A. W. Rosenbluth, M. N. Rosenbluth *et al.*, J. Chem. Phys. **21**, 1087 (1953).
[2] B. J. Alder and T. E. Wainwright, in *Proceedings of the International Symposium on Statistical Mechanics Theory of Transport Processes*, edited by I. Progigine (Wiley, New York, 1958), p. 97.
[3] A. Rahman, Phys. Rev. A **136**, A405 (1964).
[4] B. J. Berne, in *Physical Chemistry: An Advanced Treatise*, edited by H. Eyring (Academic, New York, 1971), Vol. VIIIB, Chap. 9, p. 539.
[5] J. B. Anderson, J. Chem. Phys. **63**, 1499 (1975).
[6] J. B. Anderson, J. Chem. Phys. **65**, 4121 (1976).
[7] J. B. Anderson, J. Chem. Phys. **73**, 3897 (1980).
[8] R. P. Feynman and A. Hibbs, *Quantum Mechanics and Path Integrals* (McGraw–Hill, New York, 1965).
[9] H. F. Jordon, Phys. Rev. **171**, 128 (1968).
[10] M. Parinello and A. Rahman, J. Chem. Phys. **80**, 860 (1984).
[11] R. P. Feynman, Int. J. Theor. Phys. **21**, 467 (1982).
[12] V. S. Filinov, Nucl. Phys. B **271**, 717 (1986).
[13] J. D. Doll, D. L. Freeman, and M. J. Gillan, Chem. Phys. Lett. **143**, 277 (1988).
[14] J. D. Doll, D. L. Freeman, and M. J. Gillan, J. Chem. Phys. **89**, 5753 (1988).
[15] N. Makri and W. H. Miller, J. Chem. Phys. **89**, 2170 (1988).
[16] C. H. Mak and D. Chandler, Phys. Rev. A **41**, 5709 (1990).
[17] C. H. Mak and D. Chandler, Phys. Rev. A **44**, 2352 (1991).
[18] M. Topaler and N. Makri, Chem. Phys. Lett. **210**, 285 (1993).
[19] N. Makri, Chem. Phys. Lett. **193**, 435 (1992).
[20] N. Makri, J. Chem. Phys. **97**, 2417 (1993).
[21] C. H. Mak, Phys. Rev. Lett. **68**, 899 (1992).
[22] R. Egger and C. H. Mak, Phys. Rev. B **50**, 15210 (1994).
[23] C. H. Mak and R. Egger, J. Chem. Phys. **110**, 12 (1999).
[24] R. Egger, L. Muhlbacher, and C. H. Mak, Phys. Rev. E **61**, 5961 (2000).
[25] W. H. Miller, J. Chem. Phys. **53**, 3578 (1970).
[26] M. F. Herman and E. Kluk, Chem. Phys. **91**, 27 (1984).
[27] E. J. Heller, J. Chem. Phys. **94**, 2723 (1991).
[28] K. G. Kay, J. Chem. Phys. **100**, 4377 (1994).
[29] F. Grossman and A. L. Xavier, Phys. Lett. A **243**, 243 (1998).

[30] X. Sun and W. H. Miller, J. Chem. Phys. **110**, 6635 (1999).
[31] J. Cao and G. A. Voth, J. Chem. Phys. **100**, 5093 (1994).
[32] J. Cao and G. A. Voth, J. Chem. Phys. **100**, 5106 (1994).
[33] J. Cao and G. A. Voth, J. Chem. Phys. **101**, 6157 (1994).
[34] C. H. Mak and R. Egger, Adv. Chem. Phys. **93**, 39 (1996).
[35] E. Gallicchio and B. J. Berne, J. Chem. Phys. **101**, 9909 (1994).
[36] E. Gallicchio and B. J. Berne, J. Chem. Phys. **105**, 7064 (1996).
[37] E. Gallicchio, S. A. Egorov, and B. J. Berne, J. Chem. Phys. **107**, 9312 (1997).
[38] E. Gallicchio, S. A. Egorov, and B. J. Berne, J. Chem. Phys. **109**, 7745 (1998).
[39] E. Rabani, G. Krilov, and B. J. Berne, J. Chem. Phys. **112**, 2605 (2000).
[40] G. Krilov and B. J. Berne, J. Chem. Phys. **111**, 9147 (1999).
[41] D. Kim, J. D. Doll, and D. L. Freeman, J. Chem. Phys. **108**, 3871 (1998).
[42] D. Thirumalai and B. J. Berne, J. Chem. Phys. **81**, 2512 (1984).
[43] D. Thirumalai, E. J. Bruskin, and B. J. Berne, J. Chem. Phys. **79**, 5063 (1983).
[44] B. J. Berne and D. Thirumalai, Annu. Rev. Phys. Chem. **37**, 401 (1986).
[45] E. C. Behrman and P. G. Wolynes, J. Chem. Phys. **83**, 5863 (1985).
[46] L. P. Kadanoff and G. Baym, *Quantum Statistical Mechanics* (Benjamin, New York, 1962).
[47] M. E. Tuckerman and B. J. Berne, J. Chem. Phys. **99**, 2796 (1983).
[48] R. Zwanzig, J. Stat. Phys. **9**, 215 (1973).
[49] R. P. Feynman and F. L. Vernon, Ann. Phys. (N.Y.) **24**, 118 (1963).
[50] U. Weiss, *Quantum Dissipative Systems* (World Scientific, Singapore, 1999).
[51] M. F. Trotter, Proc. Am. Math. Soc. **10**, 545 (1959).
[52] A. M. Ferrenberg and R. H. Swendsen, Phys. Rev. Lett. **63**, 1195 (1989).
[53] G. M. Torrie and J. P. Valleau, Chem. Phys. Lett. **28**, 578 (1974).
[54] N. Chakrabarti, T. Carrington, Jr., and B. Roux, Chem. Phys. Lett. **293**, 209 (1998).
[55] M. Topaler and N. Makri, J. Chem. Phys. **101**, 7500 (1994).
[56] G. Baym and D. Mermin, J. Math. Phys. **2**, 232 (1961).
[57] J. E. Gubernatis, M. Jarrell, R. N. Silver, and D. S. Sivia, Phys. Rev. B **44**, 6011 (1991).
[58] *Maximum Entropy and Bayesian Methods*, edited by J. Skilling (Kluwer, Dordrecht, 1989).
[59] M. Jarrell and J. E. Gubernatis, Phys. Rep. **269**, 133 (1996).
[60] C. L. Lawson and R. J. Hanson, *Solving Least Squares Problems* (Prentice–Hall, Englewood Cliffs, NJ, 1974).
[61] K. Miller, SIAM (Soc. Ind. Appl. Math.) J. Math. Anal. **1**, 52 (1970).
[62] R. K. Bryan, Eur. Biophys. J. **18**, 165 (1990).
[63] B. J. Berne, M. E. Tuckerman, J. E. Straub, and A. L. R. Bug, J. Chem. Phys. **93**, 5084 (1990).
[64] J. S. Bader and B. J. Berne, J. Chem. Phys. **100**, 8359 (1994).